Aalborg Universitet

AALBORG UNIVERSITY
DENMARK

Short-Range UWB Wireless Channel Measurement in Industrial Environments

Razzaghpour, Mohammad; Adeogun, Ramoni Ojekunle; Rodriguez, Ignacio; Berardinelli, Gilberto; Mogensen, Rasmus Suhr; Pedersen, Troels; E. Mogensen, Preben; Sørensen, Troels Bundgaard

Published in:
The 15th International Conference on Wireless and Mobile Computing, Networking and Communications (WiMob)

DOI (link to publication from Publisher):
10.1109/WiMOB.2019.8923145

Publication date:
2019

Document Version
Accepted author manuscript, peer reviewed version

Link to publication from Aalborg University

Citation for published version (APA):
Razzaghpour, M., Adeogun, R. O., Rodriguez, I., Berardinelli, G., Mogensen, R. S., Pedersen, T., E. Mogensen, P., & Sørensen, T. B. (2019). Short-Range UWB Wireless Channel Measurement in Industrial Environments. In *The 15th International Conference on Wireless and Mobile Computing, Networking and Communications (WiMob)* (pp. 1-6). Article 8923145 IEEE. https://doi.org/10.1109/WiMOB.2019.8923145

General rights
Copyright and moral rights for the publications made accessible in the public portal are retained by the authors and/or other copyright owners and it is a condition of accessing publications that users recognise and abide by the legal requirements associated with these rights.

- Users may download and print one copy of any publication from the public portal for the purpose of private study or research.
- You may not further distribute the material or use it for any profit-making activity or commercial gain
- You may freely distribute the URL identifying the publication in the public portal -

Take down policy
If you believe that this document breaches copyright please contact us at vbn@aub.aau.dk providing details, and we will remove access to the work immediately and investigate your claim.

Short-Range UWB Wireless Channel Measurement in Industrial Environments

Mohammad Razzaghpour[(1)], Ramoni Adeogun[(1)], Ignacio Rodriguez[(1)], Gilberto Berardinelli[(1)],
Rasmus S. Mogensen[(1)], Troels Pedersen[(1)], Preben Mogensen[(1,2)], Troels B. Sørensen[(1)]
[(1)] *Department of Electronic Systems, Aalborg University, Denmark*
[(2)] *Nokia Bell Labs, Aalborg, Denmark*
E-mail:{mor, ra, irl, gb, rsm, troels, pm, tbs}@es.aau.dk

***Abstract*—This paper presents the results of wireless channel measurement campaign in the 3 GHz to 8 GHz frequency range. The measurements were performed with focus on the short-range with a transmitter-receiver separation distance less than 9 m in two typical industrial environments: a low clutter density manufacturing space, and a high clutter density one. We analyzed the statistical properties of the most important temporal and large-scale propagation characteristics including total received energy, path loss exponent, maximum excess delay (MED) and root mean square (RMS) delay spread based on the measurements. Statistical models for the RMS delay spread and MED are also presented using the log-normal and Gamma distributions.**

***Keywords*-Measurements, Industry 4.0, short-range, UWB, path loss, maximum excess delay, RMS delay spread.**

I. Introduction

The emerging fourth industrial revolution - Industry 4.0, requires wireless communication links with up to 0.1 ms latency and a wired-like 10^{-9} reliability [1]. Compared to transmission over wired links, reliable wireless communications is more challenging due to time-varying multipath fading [2]. The industrial environments with large metallic machinery and concrete structures may create more challenging propagation conditions than non-industrial environments like urban or indoor office spaces, which may compromise the achievement of the desired levels of latency and reliability with wireless links [3]. Thus, characterization of the behavior of radio propagation channel is a crucial step in the design of ultra reliable low latency communication systems for future smart factories.

Recently, a combination of variants of OFDM and ultra wideband (UWB) radio system has been identified as a potential enabler for short-range reliable wireless connectivity in real-time industrial applications [1]. In OFDM systems, the cyclic prefix (CP) plays the crucial role of eliminating both inter-symbol interference and inter-carrier interference resulting from the multipath nature of the radio channel. To achieve this goal, the CP length must be chosen carefully with respect to the delay spread of the multipath channel [4]. Hence, it is vital to understand the delay spread characteristics of the industrial channels in addition to other temporal and large-scale fading characteristics.

In the context of multipath radio channel characteristics in industrial scenarios, literature is quite limited. In [5], measurements in the frequency range of 800 MHz to 4 GHz with access points at 6 m and terminal nodes at 2 m were presented for a wood processing factory. The work in [6] investigated small-scale fading statistics and RMS delay spread for two factory halls using measurements in the frequency range of 3.1 GHz to 10.6 GHz and 3.1 GHz to 5.5 GHz. In [7], the authors evaluated the measured power delay profile for three different industrial indoor environments in the frequency range of 800 MHz to 2.7 GHz. The results showed the effects of the highly reflective scatterers present in industrial environments. In [8], the authors presented results of channel measurements in an indoor office and industrial environment using a time domain setup which allows measurements from 3.1 GHz to 10.6 GHz. Large scale path-loss exponent, shadowing, small scale fading and RMS delay spread were reported. In [9], the authors carried out wide-band directional channel measurements at 5.2 GHz in two industrial scenarios and characterized the temporal, azimuthal and Doppler characteristics of the channel under line-of-sight (LOS) and non-line-of-sight (NLOS) conditions. More recently, The National Institute of Standards and Technology (NIST) reported a number of wide-band measurements in many different typical industrial environments, exploring path loss, delay spread, and K-factor at of 2.25 GHz and 5.4 GHz in such scenarios [10].

In order to get an insight into the specific UWB short-range propagation characteristics of industrial wireless scenarios, we conducted a dedicated measurement campaign in two factory halls with different clutter density properties (low and high) at the Smart Production Lab at Aalborg University, Denmark. This paper presents a summary of the results of the extensive high resolution ultra-wideband channel measurement campaign, focusing on the short-range (i.e. distance between TX and RX lower than 9 m), in LoS and NLoS conditions, at the two aforementioned industrial environments. Measurements were performed by frequency sounding in the range from 3 GHz to 8 GHz. We further analyzed and characterized RMS delay spread, MED, path loss exponent, and total received energy using both least squares fitting and statistical modeling.

The remainder of the paper is organized as follows: Section II presents a description of the measurement campaign.

(a) A view of Lab 1, low clutter density space (LCD).

(b) A view of Lab 2, high clutter density (HCD).

Fig. 1: Smart Production Labs.

No. of instances	Lab 1	Lab 2	**Total**
LOS	71	36	107
NLOS	27	59	86
Total	98	95	193

TABLE I: Number of instances in different state

Section III summarizes the processing applied on the measurements. Results and discussions are presented in Section IV. Finally, conclusions are drawn in Section V.

II. Measurement Campaign

The measurements reported in this paper were performed at the Smart Production Lab, at the Department of Mechanical and Manufacturing Engineering, at Aalborg University. Fig. 1 provides a visual overview of two different factory halls considered in the study - which will be refereed to as Lab 1 and Lab 2 in the rest of the paper. As a further reference on the scenario, an earlier measurement have also been performed in these industrial labs [3], addressing only large-scale parameters at 2.3 and 5.7 GHz.

Fig. 1a is an image from Lab 1 which is a "low clutter density" (LCD) space. It covers an area of about $41 \times 14\ m^2$ with a height of around 6 m which contains laboratory machinery, robots and a production line, surrounded by relatively large empty areas around the different production equipment. On the other hand, Fig. 1b shows an image of Lab 2 which is a "high clutter density" (HCD) space. It is slightly smaller than Lab 1 with an area of $33 \times 14m^2$ and a height of around 6 meters. It contains large metallic machinery like metal welding machines, hydraulic press, and material processing machines.

In this measurement campaign, we used the frequency sounding method to measure the channel complex frequency transfer function (i.e. $H(f)$). In this method, the radio propagation channel is considered as a bipolar RF network which $S_{12}(f)$ parameter is measured by a vector network analyzer (VNA). $S_{12}(f)$ is used to derive $H(f)$. Notice that since as we will see in the sequel, due to antenna effect there is a difference between $S_{12}(f)$ and $H(f)$ in this kind of measurements.

The VNA used in this experiment was a ZND 8.5 GHz model from Rohde & Schwarz. The VNA was calibrated by R&S ZN-Z51 automatic calibration unit. Fig. 2 shows the measurement setup comprising of an omni-directional, broadband 2 GHz to 30 GHz bi-conical antennas of type SZ-2003000/P at both the transmitting and receiving end of the set-up.

In total, channel frequency transfer functions were measured considering different links between 237 spatially distributed positions. The measurement locations were carefully selected to account for different impacts from scattering, dispersion, shadowing, and reflection. Potential deployment-specific configurations targeting future use cases of wireless connectivity in smart factories were also considered (i.e. the one illustrated in Fig. 2, emulating the case of a wireless sensor over the production line). More specifically, in Lab 1 and Lab 2, 98 and 95 positions were selected, respectively. The locations consist of 71 LOS and 27 NLOS situations in Lab 1. In Lab 2, 36 LOS and 59 NLOS measurements were collected. A summary of the number of measured instances in the two environments is given in Table I.

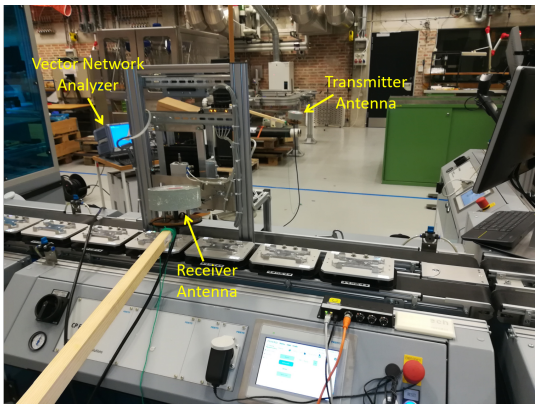

Fig. 2: Illustration of the measurement setup comprising of bi-conical antennas, a VNA and PC.

In addition, with the aim of calibration, 2 measurements with a direct cable connection to understand cable attenuation, 1 measurement with open ports to understand the noise floor and 41 measurements with free space propagation were collected. The direct cable measurements indicate that total loss in the cables is negligible (less than 0.2 dB). The open port measurement during which the VNA was not connected to an antenna or cable showed that the noise floor was about -140 dB.

In the frequency range of interest (3 GHz to 8 GHz), these antennas had a gain which varies from 0 dB to 4 dB. An appropriate calibration method could be used to compensate for the effect of antennas gain. To this end, the free space measurements were performed to estimate the antenna gains. This calibration experiment was done in a large open parking space at a time that the whole space was empty. During this free space measurements, the antenna heights was between 1 m and 2 m and the separation distance between transmitter and receiver antennas varied from 1 m to 8 m with steps of 0.5 m. Since the transmitter and receiver antenna distance was less than the break-point, we expect negligible contributions from ground reflections. The break-point is governed by $d_t = h_{Tx}.h_{Rx}.4.\pi.f/c$ which is the distance that path-loss exponent changes from 2 to 4 [11]. In the above mentioned equation, d_t is break-point distance, $h_{Tx/Rx}$ is the Tx/Rx antenna height, and f, c represents frequency and speed of light, respectively. It should be noted that during the measurements, careful evaluation of the the S_{12} and S_{11} parameters eliminates the possibility of any strong interference from other sources. We further ensured that there are no movements within the measured environments.

III. Data Processing

We present details of the analysis and computations performed on the measurements in this section. For clarity, we distinguish between the measured $S_{12}(f)$ parameter, i.e., measured frequency response incorporating both channel and antenna effects and the channel transfer function, $H(f)$, which is the equivalent of S_{12} without antenna effects. By convention, $S_{12}(f)$ can be expressed as

$$S_{12}(f) = \sqrt{G_{\rm t}(f)}H(f)\sqrt{G_{\rm r}(f)} \tag{1}$$

where $G_{\rm t}$ and $G_{\rm r}$ denote the transmitter and receiver antenna gains, respectively. For free space propagation, $S_{12}(f)$ can be obtained from Friis equation as

$$S_{12}(f) = \sqrt{G_{\rm t}(f)}\left(\frac{c}{4\pi f d}\right)\sqrt{G_{\rm r}(f)}, \tag{2}$$

where d is the distance between the transmitter and receiver. Using (1) and (2), an estimation of the transmitter/receiver antenna gain is computed through

$$G_{\rm t/r}(f) = \mathbb{E}\left\{\frac{4\pi f d S_{12}(f)}{c}\right\} \tag{3}$$

where $\mathbb{E}\{\cdot\}$ denotes the expectation operation which is performed by averaging over all free space measurements.

Since measurements were taken at discrete frequency points, i.e., $f = f_{\min} + k\Delta f; k = 0, 1, \cdots, K-1$, where $f_{\min} = 3\ GHz$ denotes the start frequency, $K = 5001$ is the number of measured point in frequency responses and $\Delta f = 1\ MHz$ is the frequency resolution, we will henceforth use a discrete index, k instead of the continuous frequency f. We compute the sampled impulse response, $h[k]; k = 0, \cdots, K-1$ via the inverse discrete Fourier transform of the transfer function.

We describe the procedure for computing the total received energy, E, RMS delay spread, $\tau_{\rm RMS}$ and maximum excess delay (MED) from the measurements. The total received energy for each measurement is computed using

$$E \triangleq \sum_{k=0}^{K-1}|h[k]|^2 = \frac{1}{K}\sum_{k=0}^{K-1}|H[k]|^2 \tag{4}$$

Substituting $H[k]$ obtained from (1) and (3) into (4) gives

$$E_{\rm FS} = \frac{1}{K}\Big(\frac{c}{4\pi d}\Big)^2\sum_{k=1}^{K}\left(\frac{1}{f_k}\right)^2, \tag{5}$$

where $f_k = f_{\min} + k\Delta f$ or equivalently,

$$E_{\rm FS}[dB] = -46.25 - 20\log_{10} d. \tag{6}$$

as the total received energy in free space. For each measurement, we compute, $\tau_{\rm RMS}$ using

$$\tau_{\rm RMS} = \sqrt{\frac{m_2}{m_0} - \left(\frac{m_1}{m_0}\right)^2} \tag{7}$$

where m_ℓ denotes the ℓth temporal moment defined as

$$m_\ell = \sum_{k=1}^{K}\tau_k^\ell |h[k]|^2; \quad \ell = 0, 1, 2, ... \tag{8}$$

We define MED as the time delay during which the received energy from a multipath falls to 20 dB below the the peak multipath energy. Thus, $\text{MED} = \tau_{20\text{dB}} - \tau_0$, where τ_0 is the delay of the first arriving path and $\tau_{20\text{dB}}$ is the maximum delay at which a multipath component is within 20 dB of the strongest path.

IV. Results and Discussion

We now present the measurements outcomes as well as discussion of investigated propagation characteristics. Due to different propagation mechanisms under LoS and NLoS conditions, measurements from both environments are separately analyzed and presented. For completeness, in some cases, the combined overview is also presented.

In Fig. 3, we present example plots of the measured industrial channel impulse response and transfer function for both LOS and NLOS in the high clutter density manufacturing space (i.e., Lab 2). As expected, the impulse response comprises of few distinct early reflections and more diffused components. Except for the first arrival in the LOS measurement, both LOS and NLOS measurements exhibit similar power level and decay rate. These two instances are measured in the same location for the transmitter antenna and receiver

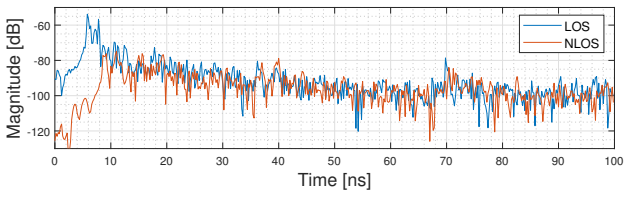

(a) Channel impulse response.

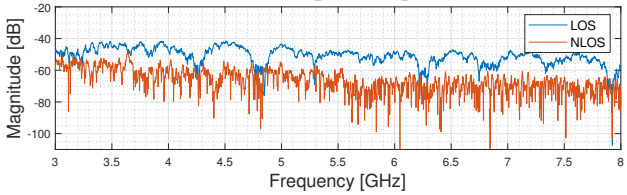

(b) Channel frequency response.

Fig. 3: Example of measured impulse response and transfer function from Lab 2.

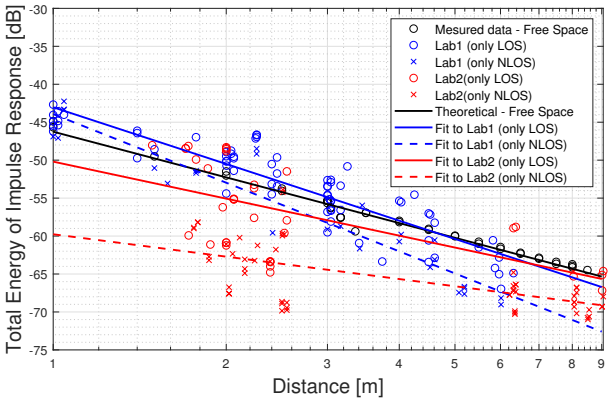

Fig. 4: Total Energy v.s. Distance, comparison between different scenarios.

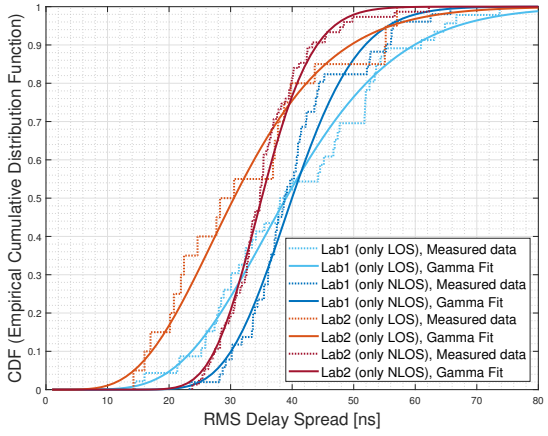

Fig. 5: CDF of RMS Delay Spread, Comparison Lab 1 and Lab 2 and fitting log-normal distribution to them.

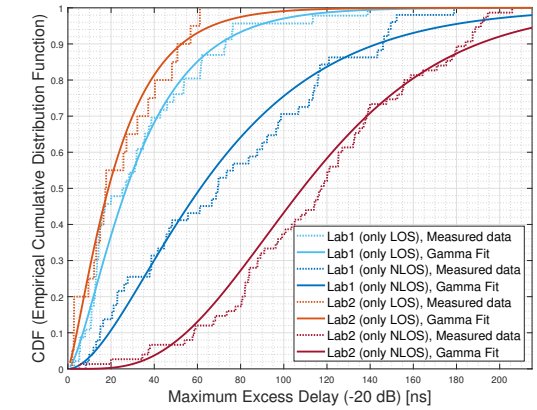

Fig. 6: CDF of MED (-20 dB), different scenarios with Gamma distribution fitting.

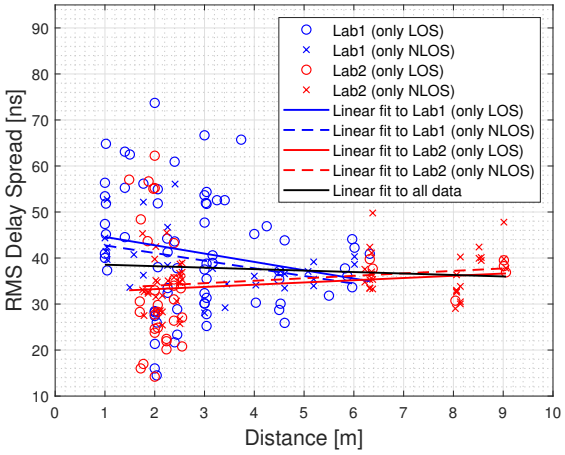

(a) RMS Delay Spread v.s. Distance, Comparison among Lab 1 and Lab 2 in LOS and NLOS states.

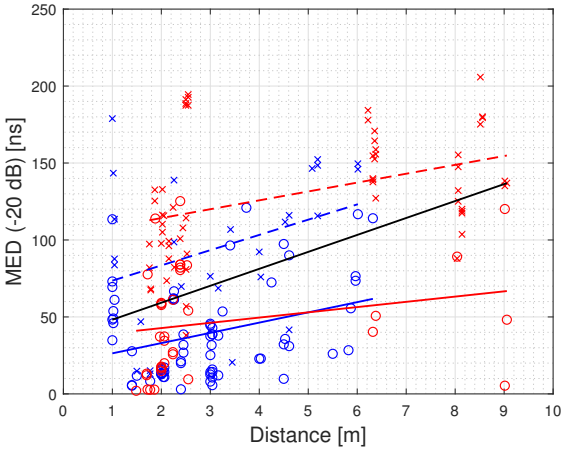

(b) MED (-20 dB) v.s. Distance, Comparison among Lab 1 and Lab 2 in LOS and NLOS states. The legends are similar to Fig. 7a.

Fig. 7: Dependency of RMS delay and MED to distance.

TABLE III: Parameters of fitted distribution

Scenario		τ_{RMS}						MED (-20 dB)					
		$90\%ile$ (ns)	Log-Normal Fit			Gamma Fit		$90\%ile$ (ns)	Log-Normal Fit			Gamma Fit	
			μ (ns)	σ (ns)	AIC	α	β (ns)	AIC	μ (ns)	σ (ns)	AIC	α	β (ns)	AIC
Lab 1	only LOS	60	3.64	0.37	377	8.00	5.08	375	73	3.18	0.88	413	1.57	21.66	415
	only NLOS	56	3.68	0.21	364	22.47	1.81	366	146	4.02	0.83	539	1.96	37.36	532
	both LOS and NLOS	56	3.66	0.30	760	12.17	3.34	757	117	3.62	0.94	979	1.46	37.27	975
Lab 2	only LOS	55	3.39	0.42	160	6.22	5.19	160	54	2.78	1.08	174	1.33	18.41	171
	only NLOS	43	3.55	0.18	493	29.39	1.21	496	184	4.65	0.57	828	4.59	25.51	805
	both LOS and NLOS	45	3.52	0.26	684	15.94	2.18	681	179	4.27	1.04	1090	1.71	57.37	1052
both labs	only LOS	55	3.57	0.40	540	6.83	5.58	538	62	3.06	0.95	587	1.45	21.46	584
	only NLOS	48	3.60	0.20	875	23.62	1.59	880	174	4.40	0.75	1406	2.62	37.87	1374
	both LOS and NLOS	53	3.59	0.29	1455	12.76	2.96	1452	153	3.94	1.04	2086	1.42	53.70	2049

Scenario		τ_{RMS}		MED (-20 dB)	
		slope (ns/m)	abscissa (ns)	slope (ns/m)	abscissa (ns)
Lab 1	only LOS	-1.81	46.39	6.65	19.69
	only NLOS	-1.66	44.41	9.91	63.66
	both LOS and NLOS	-1.80	45.94	9.24	26.96
Lab 2	only LOS	0.48	32.27	3.41	35.94
	only NLOS	0.53	32.92	5.76	102.70
	both LOS and NLOS	0.56	32.49	9.11	60.99
both labs	only LOS	-0.59	40.41	4.89	27.03
	only NLOS	0.02	36.51	7.61	86.77
	both LOS and NLOS	-0.32	38.87	11.01	37.20

TABLE IV: Parameters of linear fit to measurements of RMS delay spread v.s. distance

Scenario		PL Exponent, $-\alpha$ (dB/decade)	abscissa, β (dB)	σ (dB)
Free Space	Theoretical	2.0	-46.25	0
Lab 1	only LOS	2.48	-43.03	2.53
	only NLOS	3.00	-43.93	2.62
	both LOS and NLOS	2.69	-43.02	2.96
Lab 2	only LOS	1.62	-50.2	5.01
	only NLOS	0.98	-59.76	3.34
	both LOS and NLOS	1.56	-54.1	5.10
both labs	only LOS	2.19	-45.46	4.04
	only NLOS	1.86	-52.75	4.86
	both LOS and NLOS	2.29	-47.43	5.23

TABLE II: Parameters of linear fit to measurements of Total Energy v.s. Distance

antenna. In both cases, the transmitter-receiver separation and transmitter height was 1.7 m and 2 m, respectively. However, the Rx height for LOS and NLOS were 2 m and 0.25 m respectively.

We show the distance dependency of total energy computed from the measurements in Fig. 4 where we plot the computed energy and corresponding fitted lines. The fitted lines are obtained by calculating values of α and β for the best fit to the measurements using the same model for path loss given in [12]. We can apply this path loss model because as mentioned in equation (4), the total received energy is equivalent to the average of minus of path loss.

$$E = \beta + 10.\alpha.\log_{10}(d) + X_0 \tag{9}$$

where d is the transmitter to receiver distance and X_0 is a random variable with zero mean and standard deviation, σ. Notice that in equation (9), α is the negative of path loss exponent. In all measurements, the total energy decreases with increasing distance. However, the slope and intercept of the fits differ for Lab 1 and Lab 2 as well as for LOS and NLOS measurements. For instance, while Lab 1 shows higher total energy than theoretical free space calculation at distances below 4 m, the total energy in Lab 2 is less than free space at all distances. A plausible explanation is that, in the low clutter density environment, the received energy is more than free space due to several multipath components which in total convey more energy than the only one LOS component in the case of free space. On the other hand, blockage due to the high density of clutters in Lab 2 decreases the amount of energy from both LOS and multipath components and hence, the smaller receiver energy at all distances. A summary of the values of slope and abscissa of fitted lines as well as the standard deviation (σ) of X_0 is shown in Table II.

We present empirical cumulative distribution functions (CDF) of the time dispersion characteristics - RMS delay spread and MED in Fig. 5 and Fig. 6, respectively. Fig. 5 shows that the 90% percentile of RMS delay spread is approximately 60 ns (53 ns) and 48 ns (43 ns) under LOS (NLOS) conditions in Lab 1 and Lab 2, respectively.

Similarly, the CDF of MEDs obtained from all measurements for both LOS and NLOS is shown in Fig. 6. The mean MED in LOS (NLOS) is approximately 20 ns (62 ns) and 18 ns (117 ns) for Lab 1 and Lab 2 measurements, respectively. We also observe that both Gamma and log-normal distributions fitted appropriately to the empirical CDFs. The parameters of the distributions for both RMS delay spread and MED are shown Table III. The Akaike information criterion (AIC) is also presented as a measure of the goodness of these fits. The AIC values indicate negligible difference between the goodness of fits for both distributions.

It is worth to mention that opposite trends are observed for NLOS conditions in Figs. 5 and 6. While in Fig. 5, Lab 2 presents largest delay than Lab 1 in terms of NLOS RMS delay spread; in Fig. 6, for the MED, Lab 2 shows smaller delay values as compared to Lab 1. This should be carefully taken in consideration when designing a OFDM-based system in terms of either RMS delay spread or MED [4], as it would lead to different scenario-specific designs. Further attention will be focused on this issue in future studies, but a possible explanation for the different trends observed in terms of MED can be: 1) that there are some fundamental scenario-specific differences in terms of channel impulse response (i.e. dense multipath components in the tails), or 2) the threshold selected for the MED computation (which was fixed to 20 dB, as it has been widely used and set as almost a standard reference in the

literature) has a big impact on the MED estimation outcome. A sensitivity analysis of the impact of the MED threshold at different SNRs will be done in future studies.

Finally, Fig. 7 investigates the dependency of MED and RMS delay spread with distance. Fig. 7a depicts that the RMS delay spread, which changes from 14 ns to 74 ns, has little dependency with distance. This is also true in the case of categorizing by Lab 1, Lab 2, LOS, or NLOS instances. This is, in general, well aligned with the previous reports from literature such as, for example, the one in [6]. Fig. 7b shows that MED (-20 dB) increases with distance. Dependency of MED and distance should be carefully studied. As in the above, if the OFDM system design is based on MED instead of on RMS delay spread, one could reach to the conclusion that the cyclic prefix should be distance-dependent. As a reference, in Table IV, the slope and abscissa of fitted lines are shown.

V. Conclusions

Short-range industrial wireless channel measurements have been conducted in two typical industrial environments: a low clutter density factory hall and a high clutter density manufacturing space, considering the UWB frequency range from 3 GHz to 8 GHz. Statistical properties and distance-dependency of the RMS delay spread, maximum excess delay, path loss exponent, and total received energy have been studied. Results showed that the 90% percentile of RMS delay spread and MED in the considered short-range industrial environments can be up to 53 ns and 153 ns, respectively. The total energy and MED decreases and increases with distance, respectively. No significant dependency between RMS delay spread and distance is observed. Both Gamma and log-normal distributions yielded reasonable fits to the measured MED and RMS delay spread.The results and observations given along the study are useful for short-range UWB system design. The stochastic models provided are useful for implementation of wireless industrial network simulators.

VI. Acknowledgment

The authors would like to express their gratitude to the Robotic and Automation research group at the Department of Mechanical and Manufacturing Engineering, Aalborg University, for granting the permission to access to their industrial lab facilities. The authors would also like to thank Rohde & Schwarz for providing the vector network analyzer. The authors would also like to express their gratitude to Ali Karimidehkordi and Renato Barbosa Abreu from the Department of Electronic Systems, Aalborg University, for their collaborations during the execution of the measurement campaign.

References

[1] G. Berardinelli, N. H. Mahmood, I. Rodriguez, and P. Mogensen, "Beyond 5G wireless IRT for industry 4.0: Design principles and spectrum aspects," in *2018 IEEE Globecom Workshops (GC Wkshps)*, Dec. 2018, pp. 1–6.

[2] W. C. Jakes and D. C. Cox, *Microwave mobile communications*. Wiley-IEEE Press, 1994.

[3] D. A. Wassie, I. Rodriguez, G. Berardinelli, F. M. L. Tavares, T. B. Sorensen, and P. Mogensen, "Radio propagation analysis of industrial scenarios within the context of ultra-reliable communication," in *2018 IEEE 87th Veh. Tech. Conf. (VTC Spring)*, Jun. 2018, pp. 1–6.

[4] H. Steendam and M. Moeneclaey, "Analysis and optimization of the performance of OFDM on frequency-selective time-selective fading channels," *IEEE Transactions on Communications*, vol. 47, no. 12, pp. 1811–1819, Dec. 1999.

[5] E. Tanghe, W. Joseph, J. De Bruyne, L. Verloock, and L. Martens, "The industrial indoor channel: Statistical analysis of the power delay profile," *AEU-Inter. Journal of Electron. and Commun.*, vol. 64, no. 9, pp. 806–812, 2010.

[6] J. Karedal, S. Wyne, P. Almers, F. Tufvesson, and A. F. Molisch, "A measurement-based statistical model for industrial ultra-wideband channels," *IEEE Transactions on Wireless Communications*, vol. 6, no. 8, pp. 3028–3037, August 2007.

[7] Y. Ai, M. Cheffena, and Q. Li, "Power delay profile analysis and modeling of industrial indoor channels," in *2015 9th European Conf. on Antenn. and Prop. (EuCAP)*, Apr. 2015, pp. 1–5.

[8] Z. Irahhauten, G. J. M. Janssen, H. Nikookar, A. Yarovoy, and L. P. Ligthart, "UWB channel measurements and results for office and industrial environments," in *2006 IEEE International Conference on Ultra-Wideband*, Sep. 2006, pp. 225–230.

[9] D. Hampicke, A. Richter, A. Schneider, G. Sommerkorn, R. S. Thoma, and U. Trautwein, "Characterization of the directional mobile radio channel in industrial scenarios, based on wideband propagation measurements," in *Gateway to 21st Century Communications Village. VTC 1999-Fall. IEEE VTS 50th Vehicular Technology Conference (Cat. No.99CH36324)*, vol. 4, Sep. 1999, pp. 2258–2262 vol.4.

[10] R. Candell, C. A. Remley, J. T. Quimby, D. R. Novotny, A. Curtin, P. B. Papazian, G. H. Koepke, J. Diener, and M. T. Hany, "Industrial wireless systems: Radio propagation measurements," Tech. Rep., 2017.

[11] K. Siwiak and D. McKeown, *Ultra-wideband Radio Technology*. Wiley, 2005.

[12] T. S. Rappaport *et al.*, *Wireless communications: principles and practice*. prentice hall PTR New Jersey, 1996.